NeuroImage 201 (2019) 116036

Contents lists available at ScienceDirect

NeuroImage

journal homepage: www.elsevier.com/locate/neuroimage

State-unspecific patterns of whole-brain functional connectivity from resting and multiple task states predict stable individual traits

Yu Takagi [a,b,c,d,e,*,1], Jun-ichiro Hirayama [f,a,**], Saori C. Tanaka [a,***]

[a] ATR Brain Information Communication Research Laboratory Group, Kyoto, Japan
[b] Department of Psychiatry, Oxford Centre for Human Brain Activity, University of Oxford, Oxford, UK
[c] Department of Neuropsychiatry, Graduate School of Medicine, The University of Tokyo, Tokyo, Japan
[d] Graduate School of Information Science, Nara Institute of Science and Technology, Nara, 630-0192, Japan
[e] Japan Society for the Promotion of Science, Tokyo, 102-0083, Japan
[f] RIKEN Center for Advanced Intelligence Project, Tokyo, 103-0027, Japan

ARTICLE INFO

Keywords:
Functional connectivity fMRI
Machine learning
Human connectome project
Common functional connectivity pattern

ABSTRACT

An increasing number of functional magnetic resonance imaging (fMRI) studies have revealed potential neural substrates of individual differences in diverse types of brain function and dysfunction. Although most previous studies have inherently focused on state-specific characterizations of brain networks and their functions, several recent studies reported on the potential state-unspecific nature of functional brain networks, such as global similarities across different experimental conditions or *states*, including both task and resting states. However, no previous studies have carried out direct, systematic characterizations of state-unspecific brain networks, or their functional implications. Here, we quantitatively identified several modes of state-unspecific individual variations in whole-brain functional connectivity patterns, called "Common Neural Modes" (CNMs), from a large-scale fMRI database including eight task/resting states. Furthermore, we tested how CNMs accounted for variability in individual cognitive measures. The results revealed that three CNMs were robustly extracted under various dimensions of features used. Each of these CNMs was preferentially correlated with different aspects of representative cognitive measures, reflecting stable individual traits. Importantly, the association between CNMs and cognitive measures emerged from brain connectivity data alone ("unsupervised"), whereas previous related studies have explicitly used both connectivity and cognitive measures to build their prediction models ("supervised"). The three CNMs were also able to predict several life outcomes, including income and life satisfaction, and achieved the highest level of performance when combined with a conventional cognitive measure. Our findings highlight the importance of state-unspecific brain networks in characterizing fundamental individual variation.

1. Introduction

An increasing number of functional magnetic resonance imaging (fMRI) studies have revealed the neural substrates of individual differences by investigating the variability in whole-brain co-activation patterns (Dubois and Adolphs, 2016). The degree of co-activation between different brain regions of interest (ROIs), often referred to as functional connectivity (FC), is typically measured by the correlation of blood-oxygen-level-dependent (BOLD) signals averaged within each ROI. Brain regions that co-activate under a certain experimental condition constitute a functional "network" (with each pair-wise FC being considered an "edge'') as exemplified by the default mode network (DMN) (Raichle, 2015). The characteristics of FC patterns and networks have been associated with a wide variety of individual differences in cognition and behavior, including cognitive abilities (Finn et al., 2015; Hearne et al., 2016; Smith et al., 2015), personality (Dubois et al., 2018), sustained attention ability (Rosenberg et al., 2016), emotional sensitivity (Modi et al., 2015; Takagi et al., 2018) and psychiatric disorders (Fox and

* Corresponding author. ATR Brain Information Communication Research Laboratory Group, Kyoto, Japan.
** Corresponding author. RIKEN Center for Advanced Intelligence Project, Tokyo, 103-0027, Japan.
*** Corresponding author.
E-mail addresses: yu.takagi@atr.jp (Y. Takagi), jun-ichiro.hirayama@riken.jp (J.-i. Hirayama), xsaori@atr.jp (S.C. Tanaka).
[1] **Lead contact.** yu.takagi@atr.jp (Yu Takagi).

https://doi.org/10.1016/j.neuroimage.2019.116036
Received 21 January 2019; Received in revised form 27 June 2019; Accepted 17 July 2019
Available online 18 July 2019

Greicius, 2010; Takagi et al., 2017).

Most of these previous findings are essentially "state-specific'' because the networks were defined under a particular state when a subject is performing a specific cognitive or emotional task, or during rest. The resting state has attracted particular attention because it potentially reflects many types of individual differences and can be measured easily (Dubois and Adolphs, 2016). For example, Smith et al. (2015) revealed that a small number of linear factors ("modes") underlying individuals' whole-brain resting-state FC patterns can simultaneously explain diverse ranges of individual differences (Smith et al., 2015). They defined each mode by explicitly maximizing the correlation of linear factors (i.e., canonical correlations) between whole brain FC patterns and a wide variety of cognitive measures. It is noteworthy that Geerligs et al. (2015) demonstrated the relationship between individual differences and FC patterns may substantially change across different states and thus previous findings may not generalize to other states.

However, emerging evidence suggests that more fundamental, "state-unspecific" brain networks exist in the brain (Cole et al., 2014; Finn et al., 2015; Tavor et al., 2016). Cole et al. (2014) reported that the average FC patterns of a number of subjects exhibit a high degree of global similarity among different states, including at rest. Finn et al. (2015) reported that individual FC patterns were also generally similar across various task and resting states. Furthermore, Tavor et al. (2016) revealed that an individual's brain activity during a task state can be predicted from the individual's resting-state FC pattern. These findings strongly implicate the existence of state-unspecific brain networks. More recent reports (e.g., Rosenberg et al., 2016; Takagi et al., 2018) also suggest that some brain networks or modes can be generalized across states, emphasizing their possible relevance to the basic traits of individuals. However, none of these previous studies has explicitly identified state-unspecific brain networks or quantitatively investigated their functional relevance to individual differences. This is in part due to a lack of methods for objectively defining state-unspecific brain networks or their modes.

Here, we propose a novel systematic approach to characterizing inter-individual variability based on identifying, for the first time, state-unspecific brain networks. Our approach is directly inspired by that of Smith et al. (2015): we combine a large-scale fMRI database from the Human Connectome Project (HCP; Van Essen et al., 2012) with a linear factor analytic method to identify the latent modes underlying individuals' FC patterns. However, unlike Smith et al. (2015) and other related studies, for the first time we incorporate multiple different states (both task and rest) from the HCP data into our identification of the networks and modes. Explicitly using multi-state data, we formalize the idea of networks being unspecific to different states under a well-defined mathematical criterion, corresponding to a machine learning (multivariate statistical analysis) method that is also new in this context. The criterion is completely different from those in previous studies that maximize co-variations or predictability between FC patterns and cognitive measure. In particular, our approach to identifying the modes is completely "unsupervised", namely, we identify the modes without any explicit use of individual cognitive measures. The resultant brain networks associated with each mode, are therefore expected to represent the fundamental characterization of state-unspecific brain networks that is invariant to specific cognitive measures incorporated in the analysis.

Specifically, we use multiset canonical correlation analysis (M-CCA) (Kettenring, 1971; Vía et al., 2007) to identify the linear latent factors of individuals' FC matrices that maximize (canonical) correlations among a number of different states, including both task and rest. As emphasized above, the correlation is maximized solely among the FC matrices of different states and thus the result does not depend on particular choices of target measures, unlike typical (pair-wise) CCA analysis (Smith et al., 2015), which maximizes correlations with cognitive measures. We refer to the resultant M-CCA modes as "common neural modes" (CNMs), emphasizing that they are based purely on neural variability rather than co-variations with target cognitive measures.

Applying M-CCA on the HCP data and with statistical validations, we identify CNMs that can be robustly extracted using our unsupervised machine-learning approach. Surprisingly, the CNMs identified turn out to have significant correlations with cognitive measures reflecting basic traits such as fluid intelligence, with emphasis on different measures among different modes. Although apparently similar, previous studies all relied on the supervised approach to relate FC patterns to cognitive measures. Our result is therefore completely novel, achieved by a new method that is conceptually very different to previous ones.

In summary, our main contributions are:

1. We provide the first quantitative and unsupervised characterization of inter-individual variability based on identifying state-unspecific brain networks and their modes (i.e., CNMs). The definition of CNMs does not depend on any cognitive measures and thus can reflect a more fundamental characterization of state-unspecific brain networks than those assessed by supervised methods.
2. To achieve this, we used a novel approach based on applying M-CCA to multiple states including both task and resting states, combined with data from a large-scale fMRI database (from the HCP).
3. We identified three CNMs that can be robustly extracted. The CNMs were correlated with different cognitive measures, and they also predicted several life outcomes, in combination with a conventional cognitive measure.
4. We investigated the spatial network patterns corresponding to each CNM and show that different brain areas are associated with each CNM. These brain areas are widely distributed rather than locally focused.

2. Materials and methods

2.1. Subjects

We used a public fMRI dataset available from the HCP 500 Subject Release (Van Essen et al., 2012) (http://humanconnectome.org/data). We excluded 1) subjects who did not have data in all eight fMRI datasets (corresponding to seven task states and one resting-state) or who were not given all cognitive scores (N = 19, subdivided into 12 categories of cognition, see *Supplementary Notes* for detailed description), and 2) subjects who exhibited substantial movement during fMRI data acquisition (see *fMRI preprocessing*). After this screening process, 406 subjects were included in the final analysis. All subjects were healthy adults (ages 22–36 years, 238 females).

2.2. MRI parameters

The fMRI data were acquired using a protocol with advanced multiband sequences. Whole-brain echo-planar scans were acquired with a 32-channel head coil on a modified 3T Siemens Skyra with repetition time = 720 ms, echo time = 33.1 ms, flip angle = 52°, bandwidth 2,290 Hz/Px, in-plane field of view = 208 × 180 mm, 72 slices, 2.0 mm isotropic voxels, with a multiband acceleration factor of 8 (Uğ;urbil et al., 2013). Data were collected over 2 days. On each day, 28 min of rest-fMRI data were collected across two runs (14 min per run; 56 min over two days), followed by 30 min of task-fMRI data collection (60 min over two days). Each of the seven task-fMRI collections was completed over two consecutive fMRI runs. Three task-fMRI (working memory, reward learning, and motor responses) data were collected on the first day. The other four types of task-fMRI (emotion perception, language processing, relational reasoning, and social cognition) data were collected on the second day. More details about the fMRI collection method were described in previous studies (Barch et al., 2013; Smith et al., 2013).

2.3. Cognitive measures

In the field of cognitive neuroscience, many previous studies have focused on the relationship between various cognitive abilities and brain

activities, because they have significant effects on our daily life. Although a number of previous studies have focused on a specific cognitive measure (e.g., working memory, fluid intelligence, sustained attention), the present study sought to investigate whether CNMs have a relationship with *any* cognitive measures in a data-driven manner. In other words, we did not make any a priori assumptions about the relationships between CNMs and various cognitive abilities, unlike conventional studies. Therefore, we used the results from all cognitive tests conducted by the HCP, including episodic memory, executive function, self-regulation, language and fluid intelligence. The original set of measures was available from the HCP database website.

When both age-adjusted and age-unadjusted versions existed for the same index, we excluded the age-unadjusted version. Some cognitive tests have many strongly correlated measures; for example, "Subjective Value for $200 at 1 month" and "Subjective Value for $200 at 6 months" in the delay discounting test. In such cases, we used only the summary measure, like "Area Under the Curve for Discounting of $200". For each cognitive test, we obtained between one and three main measures, resulting in 19 measures from 12 cognitive tests in total. Details of all cognitive tests and measures are described in the *Supplementary Notes*.

2.4. Task paradigms

The seven task-fMRI paradigms were selected to activate different neural circuitry that supports broad cognitive functions, and included emotion perception, reward learning, language processing, motor responses, relational reasoning, social cognition, and working memory (Barch et al., 2013; Cole et al., 2016). Briefly, the emotion task involved matching fearful or angry faces to a target face. The reward learning task involved a gambling task involving monetary rewards and losses. The language task involved auditory stimuli consisting of narrative stories and math problems, along with questions to be answered regarding the prior auditory stimuli. The motor task involved movement of the hands, tongue and feet. The relational reasoning task involved higher-order cognitive reasoning regarding relations among features of presented shape stimuli. The social cognition (theory of mind) task used short video clips of moving shapes that interacted in some way or moved randomly, with subjects making decisions about whether the shapes had social interactions. The working memory task involved the conventional visual 2-back and 0-back tasks.

2.5. fMRI preprocessing

Fig. 1 shows a schematic diagram of our analysis. The datasets were originally preprocessed through the HCP minimal preprocessing pipeline (Glasser et al., 2013). This pipeline includes artefact removal, motion correction and registration to standard space. T1 images were segmented into three tissue classes in Montreal Neurological Institute (MNI) space using Statistical Parametric Mapping 8 (SPM8: Wellcome Department of Cognitive Neurology, http://www.fil.ion.ucl.ac.uk/spm/software/) in MATLAB (The MathWorks, Inc., Natick, MA). First, for each subject, the framewise displacement (FD) at each scan was calculated by summing up all six head motion parameters. The "scrubbing" procedure (Power et al., 2012) then identified scans that exhibited excessive head motion based on FD volumes. Specifically, a scan was flagged if the FD exceeded 0.5 mm. The flagged scan, the preceding scan, and the two subsequent scans, were excluded from the correlation analysis below. Subjects were excluded from the subsequent analyses if less than 50% of the scans remained after this procedure for any of the eight fMRI data sets. Then, for each subject, pair-wise, interregional FC was evaluated in the following manner. We used a functional atlas defining 268 ROIs that cover the entire brain (functional atlas from Finn et al., 2015, which used the method developed by Shen et al., 2013) (this atlas can be downloaded from https://www.nitrc.org/frs/?group_id=51). The representative time course of each region was extracted by averaging the BOLD time courses of the voxels within that region. Each ROI time course was linearly regressed on the temporal fluctuations of both the white matter and the cerebrospinal fluid, as well as the six head motion parameters, whose effects were then subtracted from the original time course. The fluctuation of each tissue class was the average time course of the voxels within the corresponding mask. After within-run linear trend removal, for each subject, we calculated an FC matrix consisting of all pair-wise edges between the 268 ROIs by evaluating pair-wise temporal Pearson's correlations of BOLD signal time courses of scans, based only on the remaining scans after the scrubbing step above. As the FC matrices are symmetrical, only the strictly lower triangular part of each matrix was kept, which resulted in 35,778 ($= 268 \times 267/2$) unique entries (FC values) (Fig. 1a). For all task and resting-state fMRI data, FC matrices were calculated using the same procedure. Note that an FC matrix was obtained for every run, and those of multiple runs (RL and LR phase encoding runs) were averaged in each of the eight task or resting-state conditions.

2.6. Identifying CNMs

We identified common neural modes (CNMs) of individuals as FC patterns that robustly characterized individuals irrespective of state. Specifically, we used M-CCA (Kettenring, 1971), which extends canonical correlation analysis (CCA) (Hotelling, 1936) to more than two datasets. Both methods can be used to identify canonical variates that summarize each dataset by linear transformations. In contrast, conventional CCA maximizes correlations between a pair of canonical variates, M-CCA maximizes a scalar objective function that summarizes all pair-wise correlations among M (>2) canonical variates. M-CCA reduces to CCA when the number of datasets, M, is two. Several variants of M-CCA have been proposed, depending on how they summarize the

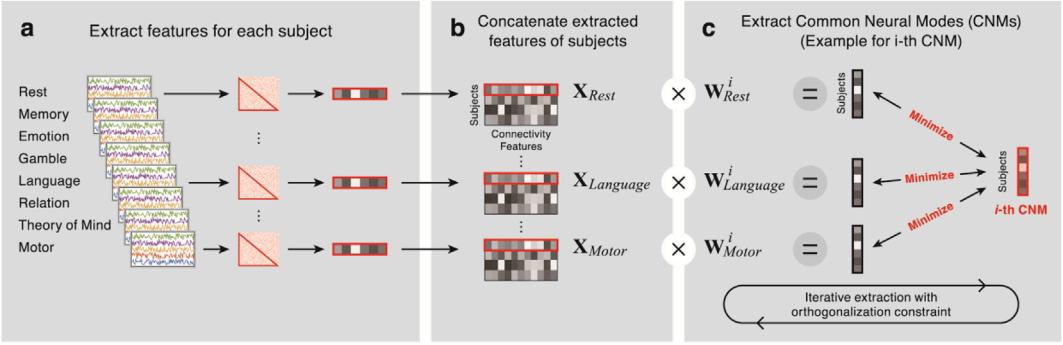

Fig. 1. Schematic diagram of the analyses. (**a**) For each subject, strictly lower triangular parts of FC matrices were extracted from each of the eight states, then vectorized. (**b**) Within each state, data for all subjects were concatenated to obtain input data matrices. (**c**) CNMs were calculated by minimizing the difference between weighted input matrices and CNMs. CNMs were iteratively calculated with the orthogonalization constraint.

pair-wise correlations into a single objective function (Kettenring, 1971). We chose the MAXVAR approach because it explicitly introduces common latent factors across different datasets (Vía et al., 2007), which can be naturally interpreted as CNMs.

Suppose that we are given M data matrices $\mathbf{X}_k \in \mathbb{R}^{N\times m_k}$, $k = 1,...,M$ (Fig. 1b), where N denotes the sample size and m_k denotes the dimensionality of the k-th data space. Each column is assumed to have zero sample mean, without loss of generality. The MAXVAR approach can then be stated as the problem of finding M weight vectors $\mathbf{w}_k$ ($k = 1,...,M$), for each of the M datasets, so that the errors between the corresponding canonical factors $\mathbf{X}_k\mathbf{w}_k$ and their grand average $\mathbf{z} \in \mathbb{R}^{N\times 1}$ is minimized. The cost function to be minimized is formally given as

$$J = \min \sum_{k=1}^{M} \mathbf{z} - \mathbf{X}_k\mathbf{w}_k^2.$$

where the minimization is performed with respect to both $\mathbf{w}_k$ and $\mathbf{z}$. To avoid trivial solutions, $\mathbf{w}_k$ and $\mathbf{z}$ are constrained to have unit Euclidean norms, and to be mutually orthogonal. The solution is given by solving a generalized eigenvalue problem. See Via et al. (2005) for more detailed information about this procedure. Solving this problem gives a set of M vectors $\mathbf{w}_k$, and CNMs are defined as the average of $\mathbf{X}_k\mathbf{w}_k$ for $k = 1, \ldots, M$ (Fig. 1c). We iteratively repeated this procedure N times, where N is the number of CNMs determined arbitrarily. The subsequent $\mathbf{z}_{n+1}$ are constrained to be orthogonalized to $\mathbf{z}_n$.

To reduce redundancy among edges, the dimensionalities of the data matrices were reduced in advance using principal components analysis (PCA). The numbers of principal components were varied between 10, 50 and 100 for calculating CNMs, and the numbers of CNMs were also varied between 10, 50 and 100, respectively. The significance of the pair-wise canonical correlations was investigated using a permutation test for individual CNMs. We first shuffled subject labels of all $\mathbf{X}_k$, then conducted M-CCA. We ran these analyses 1,000 times and obtained 1,000 instances of estimated $\mathbf{w}_k$. We then took the average of the absolute correlation coefficients between all pairs among $\mathbf{X}_k\mathbf{w}_k$ for each random dataset. Finally, we calculated the statistical significance by comparing the true averaged value of the correlation coefficient with those obtained from shuffled datasets.

2.7. Determining the number of CNMs

We evaluated the statistical significance by comparing the average value of the correlation coefficient with that obtained from 1,000 shuffled datasets. We then identified CNMs that exhibited significant p-values ($p < 0.05$) consistently across different PCA dimensions (10, 50 and 100). For the following analyses, we used only the CNMs determined by this analysis.

2.8. Interpretation of CNMs

To facilitate biological interpretation of the CNMs, we summarized FC patterns that were correlated with the first, second and third CNMs. The three CNMs were those identified as above. First, we averaged every FC value over all eight states. We then calculated absolute Pearson's correlation coefficients between three averaged CNMs and each averaged FC. To aid interpretation, only the most strongly correlated 200 edges among all 35,778 edges were kept, and these edges were further summarized using the node (ROI) labels that assign each node to one of eight representative macroscale networks (e.g., the DMN), also available with the atlas (Finn et al., 2015; see above). Specifically, we examined the number of edges between each network pairs and normalized the edge counts by the number of possible edges between that network pair. Finally, we visualized the relative numbers of edges in each of the network pairs as the thickness of the connection lines.

2.9. Relationship between CNMs and cognitive measures

To analyze how CNMs were associated with individual differences in behavior, we calculated Pearson's correlations between the CNMs and cognitive measures obtained using the HCP with various batteries. We used a rank-based inverse Gaussian transformation (der Waerden and van der Waerden, 1952), to enforce Gaussianity for each of the CNMs and cognitive measures. To reduce the risk of overfitting, we conducted all analyses in a fully cross-validated manner (Barch and Yarkoni, 2013). Specifically, we first split all the subjects into 10 disjointed subsets of subjects. The model for calculating CNMs was then obtained based on all but one set of subjects (training set) and the model was then tested on the one withheld set of subjects (test set). We repeated this procedure 10 times (10-fold cross validation), and obtained all subjects' cross-validated CNMs. We then calculated Spearman's rank correlation between these CNMs and cognitive measures across subjects.

2.10. Prediction of life outcomes using CNMs

The preceding analysis suggested that CNMs were correlated with representative cognitive measures obtained by the behavioral batteries such as fluid intelligence. Thus, we further investigated whether the CNMs can account for individual differences in the subjects' life outcomes, which are considered to be predicted by intelligence measures in the field of educational psychology (Cattell, 1963; Colom et al., 2010; Gottfredson, 1997). As a measure of life outcomes, we chose three measures: income, life satisfaction and years of education. We conducted the analysis using nested 10-fold cross validation. We first split all subjects into 10 sets of subjects, and identified CNMs based on the training set, as in the previous analysis. We then constructed a prediction model using 5-fold cross validation among the training set. We used the L1-regularized linear regression model for each iteration. The hyper-parameter λ(the regularization coefficient) was tuned by choosing the best value from $\lambda \in \{0.0001, 0.001, 0.01, 0.1\}$ based on this inner 5-fold cross validation. We finally used the hyper-parameter λ which performed the best in the inner 5-fold cross validation for predicting life outcomes of the test set. Performance was evaluated by Pearson's correlation coefficients between predicted and actual life outcomes across whole subjects.

As a comparison, we constructed a prediction model of life outcomes using cognitive measures. Here, we used number of correct answers in the Penn Progressive Matrices test, which is a representative cognitive measure of fluid intelligence and is known to be a predictor of some life outcomes. We examined whether adding the cognitive measure of fluid intelligence as explanatory variables improved the prediction performance over that obtained by CNMs only. To investigate this, we constructed a prediction model (L1-regularized linear regression) using both CNMs and fluid intelligence. These predictions were conducted in the same manner as described above for the prediction model using only CNMs.

The significance of the prediction performance in each life outcome for the models of CNM or fluid intelligence were examined using a permutation test. Specifically, we constructed 10,000 CNMs from the shuffled dataset and 10,000 from shuffled fluid intelligence. We then constructed prediction models for each life outcome using shuffled CNMs or fluid intelligence. Finally, we calculated the statistical significance by comparing the true prediction performance with that obtained from shuffled CNMs or fluid intelligence. Note that the simple correlation analysis (as we used in the previous section) is not suitable for such a combinatory analysis with both CNM and the fluid intelligence measure, and hence we used the prediction (multiple regression) model, which can properly estimate the additive explained variance of the CNMs to fluid intelligence.

The significance of the model using both CNMs and fluid intelligence was calculated by comparing the prediction performance of the model with the prediction performance of the models of shuffled fluid

intelligence and *unshuffled* CNMs 10,000 times. By fixing CNMs and shuffling only fluid intelligence, we were able to test the significance of improvement by adding fluid intelligence to the prediction model. Finally, we calculated the statistical significance by comparing improvement of the true model with that obtained from shuffled models.

2.11. Effects of the number of states used to identify CNMs

We investigated the effects of the number of states used to identify CNMs on prediction accuracy. Specifically, we conducted the same prediction analyses as above, but used a smaller number of states for constructing the CNMs. We varied the number of states for constructing the CNMs from 2 to 8. We calculated all possible combinations for each case. For example, we calculated 28 CNMs ($=\binom{8}{2}$), then constructed prediction models for all CNMs, when we estimated the prediction accuracy of two states.

2.12. Effects of the number of time-points on CNMs

We next investigated the effects of the number of time points for CNMs using two different types of datasets. First, we used four resting-state fMRI runs for CNMs (2 days $\times$ 2 runs). Second, we used four runs from different states for CNMs, for example, the first run of emotion perception, reward learning, language processing, and motor responses tasks. Because we have 4 runs of resting-state and 2 runs of 7 task-states, the number of patterns is $({}_7C_3 \times 4 \times 2 \times 2 \times 2) + ({}_7C_4 \times 2 \times 2 \times 2 \times 2) = 1{,}680$ patterns. For all states, we used the first 176 scans to balance the number of time points. Finally, by using CNMs obtained from the above two datasets, we calculated Pearson's correlation coefficients with original CNMs and predicted life outcomes.

3. Results

3.1. Identifying CNMs

We first determined the number of CNMs that exhibited significant pair-wise canonical correlations among the eight states. For any choices of the preprocessing PCA dimensionality (i.e., 10, 50, and 100), the first, second and third CNMs (namely CNM1, CNM2 and CNM3) exhibited significant overall correlations between states (where all pair-wise correlations were averaged) ($P < 0.001$ for all CNMs; 1,000 times permutation test); the other CNMs did not ($P > 0.05$; 1,000 times permutation test). We therefore focused on the top three CNMs, obtained by M-CCA on 10 PCs of edge vectors.

We also conducted several control analyses (see *Supplementary Notes*). First, the M-CCA results were highly consistent under different choices of PCA dimensions (see Supplementary Table 1). We also confirmed that the three CNMs were, in general, equally correlated with all states, and the relationship was not correlated with the scan duration of the states. Furthermore, because the number of scans differed across different states (for example, the emotion task had 176 scans, which was the lowest among all states, and the resting-state had 1,200 scans, which was the highest among all states), we investigated the effect of the number of scans on CNMs using the same number of scans for all states. Here, we used first 176 scans for all states. The results revealed that the correlations between the three original CNMs and these scan-number-matched CNMs were still strong (Pearson's $R > 0.9$ for CNM1, $R > 0.6$ for CNM2 and CNM3). In addition, to investigate the effects of the number of states on CNMs, we calculated CNMs using the same number of scans with two types of the combination of states: 1) scans from resting-states only and 2) scans from different states. We confirmed that it is important for CNMs to use various states, rather than scans from a single state (see *Supplementary Notes*). Finally, we confirmed that when we split the dataset into 10 sub sets for 10-fold cross validation in a different manner taking the HCP family structure into account (Winkler et al., 2015, 2014), we obtained consistent results.

3.2. Relationship between CNMs and cognitive measures

We then investigated which cognitive measures were correlated with each of the three CNMs. Fig. 2a, b and 2c show the distributions of the correlation coefficients between cognitive measures and CNM1, CNM2 and CNM3, respectively. CNM1 was preferentially correlated with fluid intelligence. CNM2 was correlated with various language-related measures (reading recognition and vocabulary comprehension) and self-regulation (delay discounting). CNM3 was correlated with both fluid intelligence and language-related measures.

Several control analyses were performed to further increase confidence that the relationship was robust (see *Supplementary Notes*). First, when we regressed out potential co-variations including sex, age, scanning protocols, and quality-control issues, there was almost no change in the results. We also confirmed that correlation patterns between cognitive measures and CNMs were not similar to correlation patterns between a specific PC and cognitive measure. Rather, these correlation patterns were generally equally similar to all PCs (see Supplementary Fig. 1). We further confirmed that when we apply Spearman's correlation analysis without rank-based inverse Gaussian transformation, the results do not change (see *Supplementary Notes*). Finally, although we have already exhaustively addressed head motion by regressing out from raw signals and by the scrubbing procedure, to further investigate the effects of head motion on CNMs, we calculated partial correlations between CNMs and cognitive measures. We confirmed that using partial correlation does not qualitatively change the results (see Supplementary Fig. 2).

3.3. Interpretation of CNMs

To facilitate biological interpretation of the edges underlying CNMs, we grouped the 268 ROIs into eight macroscale canonical networks (Finn et al., 2015). Fig. 1d, e and 1f show the circle plots of the edges that were correlated with CNM1, CNM2 and CNM3. The numbers of edges for each pair of macroscale regions (the MF, FP, DMN, SC-CB, MTR, V1, V2, and VAssc), normalized by the maximum possible number of edges for the pair, are presented as the thickness of the connection lines. Connection lines are colored blue within the same network and red between network pairs. Although the edges were widely distributed rather than locally focused, there were some differences in the distributions among the CNMs. Nearly half of the edges in CNM1 belonged to the networks between cortical and subcortical brain regions, including the medial frontal network and motor network. In contrast, nearly half of the edges in the CNM2 belonged to networks between the motor and visual networks. Edges including frontoparietal network and subcortical network also contributed to the CNM2. Compared with CNM1 and CNM2, edges in CNM3 belonged to a variety of networks including both the cortico-cortico and cortico-subcortical networks. It is noteworthy that the DMN had a substantial contribution to the CNM3, but did not contribute to the CNM1 or CNM2. We confirmed that the spatial interpretation above was robust under various numbers of edges chosen from all edges (see *Supplementary Notes*). We also investigated the node-level contribution by checking the degree of connectivity (Supplementary Fig. 3). The node-level results were consistent with the canonical network level network results, i.e., CNM1 was mainly related to subcortical and temporal regions, CNM2 was related to motor and visual regions, and CNM3 was related to wider regions, including subcortical, temporal and frontal regions.

3.4. Prediction of life outcomes using CNMs

We next investigated whether CNMs could predict life outcomes and complement conventional cognitive measures.

Fig. 3a, b and 3c show that prediction with CNMs alone achieved

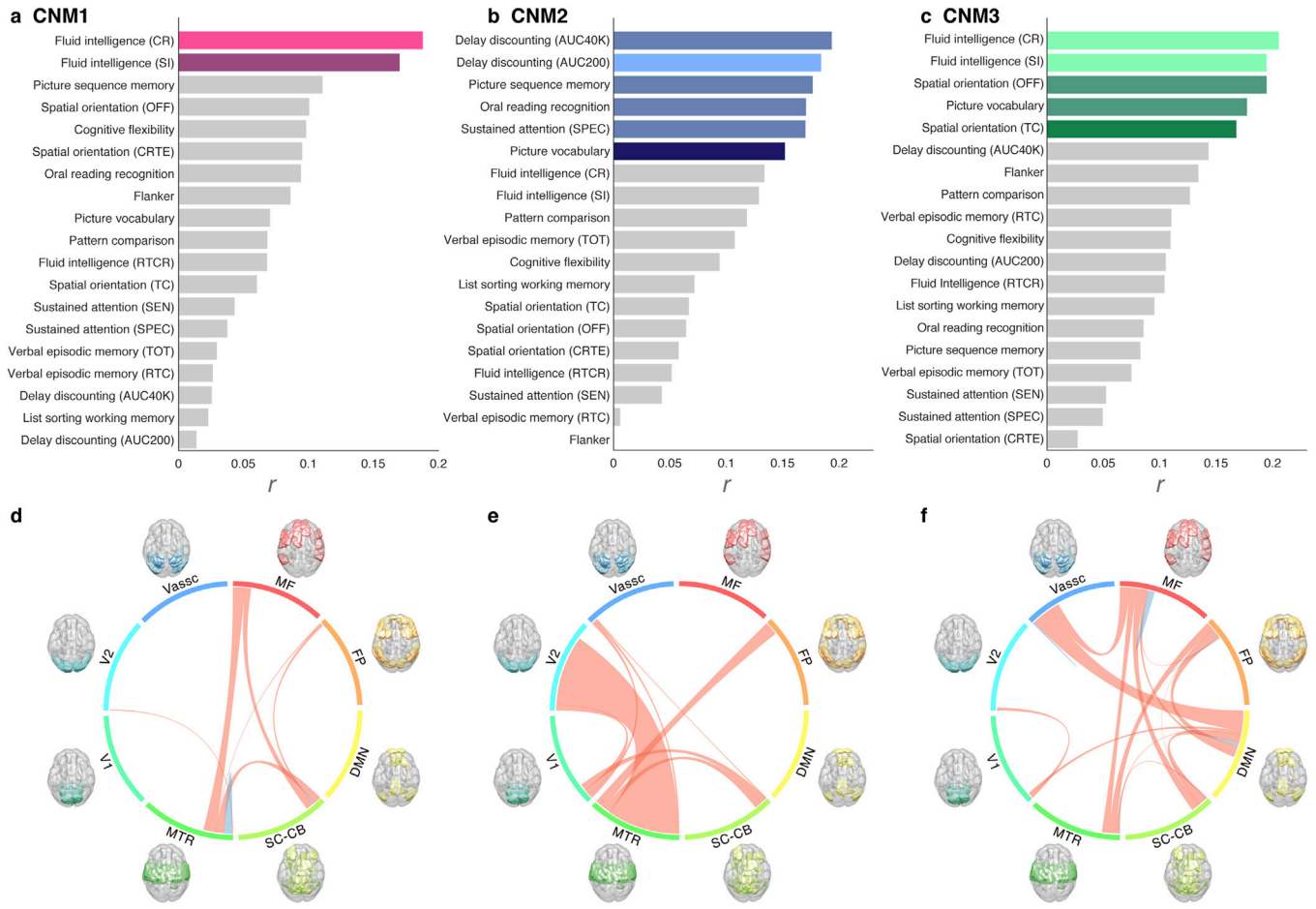

Fig. 2. Characterization of CNMs. (a-c) Absolute correlation coefficients (r) between 19 cognitive measures and (**a**) CNM1, (**b**) CNM2 and (**c**) CNM3, respectively. See *Supplementary Notes* for explanations of all abbreviations. Bars with light, medium, dark color and grey indicated different levels of significance ($P < 0.001$, $P < 0.01$, $P < 0.05$ and $P \geq 0.05$, respectively; 10,000 times permutation test; Bonferroni correction for multiple comparisons). **(d-f)** The spatial distribution of the edges was related to CNMs. The number of edges between each pair of canonical networks in **(d)** CNM1, **(e)** CNM2 and **(f)** CNM3, respectively. Canonical networks included the medial frontal (MF), frontoparietal (FP), DMN, subcortical-cerebellum (SC-CB), motor (MTR), visual I (V1), visual II (V2), and visual association (VAssc). Connection lines were colored blue within the same network and red between network pairs.

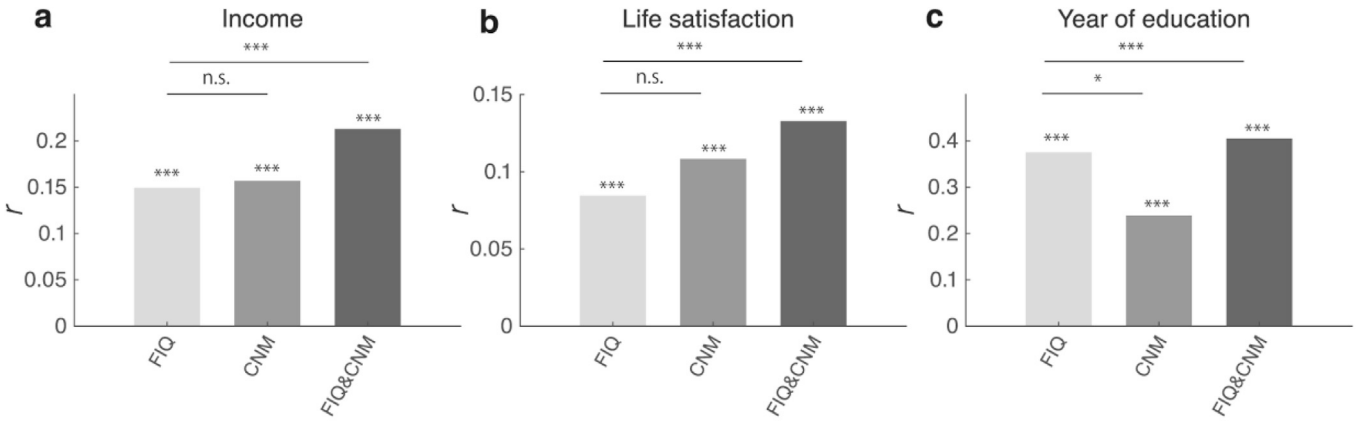

Fig. 3. Prediction performance. Cross validated prediction accuracies by the fluid intelligence (FIQ) obtained by the behavioral battery (left), the CNMs (middle) and their combination (right) for (**a**) income, (**b**) life satisfaction and (**c**) number of years of education, respectively. 10,000 times permutation test, * corresponds to $P < 0.05$, ** to $P < 0.01$, *** to $P < 0.001$, and *n.s.* to a non-significant difference, Bonferroni correction for multiple comparisons.

significant predictive value ($P < 10^{-4}$ for income and number of years of education; $P < 2.00 \times 10^{-4}$ for life satisfaction; 10,000 times permutation test). The prediction accuracies (r) achieved by the model using CNMs alone are comparable to the model using fluid intelligence for income and life satisfaction ($P = 1.00$ for both life outcomes; Steiger's z test), but slightly worse for years of education ($P = 0.039$; Steiger's z test). We also confirmed that correlations between predicted and actual subjects' life outcomes were still significant after regressing out the effect of fluid intelligence from CNMs ($P < 3.00 \times 10^{-4}$ for income; $P < 10^{-4}$ for years of education; $P < 2.00 \times 10^{-4}$ for life satisfaction; 10,000 times

permutation test). Combining both the CNMs and fluid intelligence yielded the highest performance in every case ($P < 10^{-4}$ for all income and years of education; $P < 2.00 \times 10^{-4}$ for life satisfaction; 10,000 times permutation test). Different models using whole PCs from all states or using another unsupervised method (independent components analysis [ICA]) were also tested as a comparison (see *Supplementary Notes*).

3.5. Effects of the number of states used for the CNMs

We further investigated the effects of the number of states used for identifying CNMs on prediction accuracy. Fig. 4a, b and 4c show the prediction accuracies using the CNMs with different numbers of states. These figures indicate that the more states we used, the greater accuracy we were able to achieve for predicting life outcomes. We constructed linear regression models and found that the effects of the number of states were significant for all models ($P = 8.15 \times 10^{-13}$ for income; $P = 5.71 \times 10^{-13}$ for life satisfaction; $P = 0.007$ for years of education).

3.6. Effects of the number of time-points on CNMs

We next investigate whether different cognitive states, rather than more time points, gives reliable CNMs.

For CNM1 and CNM2, we obtained higher correlations with original CNMs when we used 4 runs from different states, compared with the 4 resting-state runs. Specifically, for CNM1, all 1,680 patterns of 4 runs from different states have higher correlations than the 4 resting-state runs (Pearson's $R = 0.79 \pm 0.001$ [mean ± s.e.m] by different 4 states; $R = 0.04$ by 4 resting-state runs). For CNM2, 1,369 of the 1,680 patterns of 4 runs from different states have higher correlations for CNM2 ($R = 0.36 \pm 0.005$ by different 4 states; $R = 0.14$ by 4 resting-state runs). Conversely, for CNM3 we tended to obtain lower correlations with original CNMs when we used 4 runs from different states, compared with the 4 resting-state runs. That is, 532 of the 1,680 patterns have higher correlations ($R = 0.27 \pm 0.004$ by different 4 states; $R = 0.34$ by 4 resting-state runs).

In addition, we obtained higher prediction accuracies when we used 4 runs from different states compared to the 4 resting-state runs. Specifically, 1,435 patterns have higher correlations for income (Pearson's $R = [0.24; -0.04; -0.22]$ by 4 different states [max; mean; min]; −0.14 by 4 resting-state runs), 1,285 patterns have higher correlations for years of education ($R = [0.32; 0.11; -0.07]$ by 4 different states; 0.06 by 4 resting-state runs), and 1,655 patterns have higher correlations for life satisfaction ($R = [0.17; 0.00; -0.16]$ by 4 different states; −0.11 by 4 resting-state runs) among the 1,680 patterns.

In summary, using various states is an important component of assessing our CNMs, especially for CNM1 and CNM2, and prediction of life outcomes.

4. Discussion

In the present study, we conducted, for the first time, a quantitative analysis of inter-individual variability based on identifying state-unspecific brain networks and their associated modes (i.e. CNMs) using an unsupervised method, that is, with no explicit use of individuals' cognitive measures. We investigated the associations between CNMs and cognitive and life outcome measures. Although previous studies have suggested state-unspecific properties of FC (Cole et al., 2014; Finn et al., 2015; Tavor et al., 2016), to our knowledge, no study has defined state-unspecific networks in a quantitative manner. The CNMs were extracted by M-CCA in a fully cross-validated manner from the HCP fMRI datasets, covering a broad range of task- and resting-states. We further demonstrated that the CNMs were able to predict several life outcomes, complementing conventional behavioral batteries of fluid intelligence. We also found that the more states we used to identify CNMs, the higher accuracy we were able to achieve when predicting life outcomes. The network edges constituting those CNMs were widely distributed throughout the brain rather than being locally constrained. Importantly, no CNM dominantly reflected any particular state, such as the resting state, but each related to all states equally. Full investigation of this phenomenon will require further study.

Three CNMs were robustly extracted by M-CCA, revealing significant correlations with representative cognitive measures, especially intelligence measures such as fluid intelligence (Fig. 2). Intelligence measures are related to a wide range of cognitive functions and may predict various social outcomes, such as educational achievement, job performance, health, and longevity (Cattell, 1963; Colom et al., 2010; Gottfredson, 1997). Intelligence measures can therefore be considered to provide fundamental state-unspecific characterization of individual differences observed in behavior. In contrast, CNMs offer a possible biological basis of state-unspecific individual differences, and could be reasonably expected to exhibit some similarity with intelligence measures, which was confirmed by our analysis.

It is also noteworthy that each of the three CNMs correlated with different cognitive measures. That is, CNM1 correlated with fluid intelligence, CNM2 correlated with delay discounting and language-related measures, and CNM3 correlated with fluid intelligence, spatial orientation, and language-related measures. This suggests that these CNMs may have different biological substrates (Fig. 1d, e and 1f). Importantly, the CNMs were derived in a fully data-driven, cross-validated manner. In fact, the correlation between CNMs and these cognitive measures was non-trivial and surprising, because our definition of CNMs does not explicitly maximize correlations with these cognitive measures themselves, unlike previous related studies (Finn et al., 2015; Lerman-Sinkoff et al., 2017; Schultz and Cole, 2016) (see also below). It is noteworthy that most of these previous studies examined only one state, while we jointly analyzed multiple states, which is also an important novelty of our

Fig. 4. Relationship between the number of states used for the CNMs and prediction performance. Cross validated prediction accuracies of the CNMs obtained from different numbers of states for (**a**) income, (**b**) life satisfaction and (**c**) number of years of education, respectively. Error bars correspond to standard error of the mean.

study. The level of correlation between CNMs and cognitive measures, especially for fluid intelligence, were unfortunately not as high as those in previous studies (Finn et al., 2015; Lerman-Sinkoff et al., 2017; Schultz and Cole, 2016). However, this is a natural consequence of using an unsupervised method (M-CCA) rather than the supervised methods used in the previous studies. Our results thus shed new light on the results of previous studies from the previously-lacking viewpoint of state-unspecific brain networks; that is, the network patterns found by previous studies could in part also be interpreted as constituting such a fundamental type of brain network.

When predicting life outcomes, using only CNMs achieved higher prediction accuracies for income and life satisfaction than prediction with conventional intelligence measures alone. In contrast, conventional intelligence measures achieved better prediction of the number of years of education (Fig. 3). These results may reflect different characteristics between biologically defined measures and measures from a behavioral battery. It should be noted that combining CNMs with fluid intelligence achieved the highest prediction accuracies for all life outcomes. These results indicate that CNMs contain valuable information for predicting behavior that may not be captured by conventional intelligence measures.

Importantly, using a greater number of states to identify CNMs led to greater prediction accuracy (Fig. 4). This indicates that CNMs were more reliably extracted when performing M-CCA with a greater number of states. Our findings suggest that contrasting many different states, rather than considering any single (typically resting) state, can more reliably identify the modes that are able to predict diverse types of individual differences, especially for CNM1 and CNM2. We confirmed that CNM1 and CNM2 were extracted reliably and state-invariance was crucial based on the exhaustive comparison between CNMs obtained from single state versus varied states. It should be noted that, however, state-invariance was not crucial for obtaining CNM3. In other words, although CNM3 was derived by maximizing state invariance, state-invariance may not be the primary characterization of CNM3.

Although all three CNMs were related to the subcortical networks and motor networks, we observed some differences among them, in terms of the related canonical networks (Fig. 2d, e, 2f). CNM1, CNM2 and CNM3 were related to the medial frontal network, frontoparietal network, and both networks, respectively. Interestingly, this finding coincides with another finding that CNM1 and CNM2 captured different aspects of cognitive measures while CNM3 was somewhat intermediate.

We found that brain regions contributing to all CNMs were widely distributed rather than locally restricted. The contributions of the widespread brain regions we observed are consistent with a previous study reporting that brain regions related to intelligence were broadly distributed (Basten et al., 2015; Finn et al., 2015; Haier et al., 2009; Jung and Haier, 2007; Smith et al., 2015). Specifically, Jung and Haier (2007) used the parieto-frontal integration theory of intelligence to describe a network of frontal and parietal brain regions as the main neural basis of intelligence. Basten et al. (2015) conducted a functional meta-analysis, reporting clusters distributed across both hemispheres, located in the lateral frontal, medial frontal, parietal, and temporal cortices. In addition, Basten et al.'s (2015) structural meta-analysis revealed clusters distributed in lateral and medial frontal, temporal, and occipital cortices, and in subcortical structures. Although it is difficult to directly compare the present results with these previous studies, because CNMs consist of FC and are constructed in a different manner, it is notable that we also found relationships between CNMs and subcortical, medial-frontal, fronto-parietal and DMN regions.

As mentioned above, our study did not explicitly use cognitive measures for deriving CNMs, which is in stark contrast to previous studies that necessarily incorporated them in their models (Finn et al., 2015; Hearne et al., 2016; Smith et al., 2015, for example). This was because our main purpose was to quantitatively define the common brain components underlying individual differences, rather than investigating the sources of a specific cognitive ability by correlation or prediction analyses. Although a small number of studies have reported evidence of the state-unspecific nature of brain networks (Cole et al., 2014; Finn et al., 2015; Tavor et al., 2016), to our knowledge our study is the first to have systematically identified the state-unspecific networks and their modes in a quantitative manner.

Recent reports (e.g., Takagi et al., 2018; Rosenberg et al., 2016) suggested that some brain networks or modes can be generalized across states. We previously showed that there is a common brain network that can generalize across different states using different types of fMRI dataset including task-fMRI, resting-state fMRI from healthy participants, and resting-state fMRI from patients with psychiatric disorders (Takagi et al., 2018). In that study, we focused on "anxiety" and showed that state-, trait- and pathological-anxiety are not completely independent but has common neural substrates. Rosenberg et al. (2016) also showed that there is a common brain network related to sustained attention. Importantly, these previous studies used supervised techniques, i.e. they explicitly considered target variables (e.g., anxiety or sustained attention) and aimed to extract a common brain network related to the variable. This is a critical difference from the present study which uses an unsupervised technique. It is noteworthy that, the technique employed in the present study, M-CCA, can also be used for the datasets used in the previous study. By applying M-CCA, we can investigate whether the networks reported in the previous studies were "dominant" shared network among the other shared brain networks.

Although we focused on state-unspecific modes across various states, these modes would be expected to function in a coordinated way with other state-specific modes in any particular state. Different modes for respective states may have different abilities associated with different neural substrates, which may also cause individual differences in behavior. Thus, it would be useful in future studies to comprehensively compare the relationship between state-specific and state-unspecific modes in terms of their relationship with both cognitive measures and neural substrates. Although we found significant correlations between CNMs and cognitive measures, the effect size ($R < 0.2$) was relatively low. One reason for this was the use of an unsupervised method, as described above. However, correlations are often modest when predicting cognitive measures using FC fMRI (e.g., Dubois et al., 2018; Noble et al., 2017). Potential reasons include the typically high level of measurement noise during fMRI and the relatively small sample sizes. Future studies with larger sample sizes and signal-to-noise ratios could further improve the effect size.

In summary, we identified the modes of inter-individual variability in whole-brain functional connectivity that are stable across different states, and then quantitatively investigated their relationships with various individual differences. These components, referred to as CNMs, were identified in a fully data-driven manner using an unsupervised machine learning technique, without relying on any target cognitive measures. The CNMs were significantly correlated with representative cognitive measures as well as life outcomes. Although previous studies have suggested that potential brain networks are shared among broad states, the current study is the first to quantitatively define such networks and demonstrate that they may have a broad effect on behavior and life outcomes. We believe that the present study provides evidence that state-unspecific brain networks are related to a diverse range of behaviors and life outcomes.

Conflicts of interest

The authors declare no competing financial interests.

Acknowledgements

This work was supported by the project 'Science of personalized value development through adolescence: integration of brain, real-world, and life-course approaches' (16H06396, 16K21720, 16H06395) and 'Adolescent Mind & Self-Regulation' (23118002) from the Japan Society

for the Promotion of Science (JSPS). This study was partially conducted under the "Development of BMI Technologies for Clinical Application" of the Strategic Research Program for Brain Sciences (JP17dm0107044) supported by the Japan Agency for Medical Research and Development (AMED). SCT was supported by KAKENHI 16K01958 from JSPS. JH was supported by KAKENHI 17H06041 and 18KK0284 from JSPS. We thank Hiroshi Imamizu, Ph.D., Masahiro Yamashita, Ph.D., Ryu Ohata, Ph.D., for helpful discussions and proofreading the manuscript. We thank Mitsuo Kawato, Ph.D., Kazuo Shigemasu, Ph.D., Okito Yamashita, Ph.D., and Ayumu Yamashita, Ph.D. for helpful discussions. We thank Nobuyuki Izumihara for his support for visualization.

Appendix A. Supplementary data

Supplementary data to this article can be found online at https://doi.org/10.1016/j.neuroimage.2019.116036.

References

Barch, D.M., Burgess, G.C., Harms, M.P., Petersen, S.E., Schlaggar, B.L., Corbetta, M., Glasser, M.F., Curtiss, S., Dixit, S., Feldt, C., Nolan, D., Bryant, E., Hartley, T., Footer, O., Bjork, J.M., Poldrack, R., Smith, S., Johansen-Berg, H., Snyder, A.Z., Van Essen, D.C., 2013. Function in the human connectome: task-fMRI and individual differences in behavior. Neuroimage 80, 169–189. https://doi.org/10.1016/j.neuroimage.2013.05.033.

Barch, D.M., Yarkoni, T., 2013. Introduction to the special issue on reliability and replication in cognitive and affective neuroscience research. Cognit. Affect Behav. Neurosci. 13, 687–689. https://doi.org/10.3758/s13415-013-0201-7.

Basten, U., Hilger, K., Fiebach, C.J., 2015. Where smart brains are different: a quantitative meta-analysis of functional and structural brain imaging studies on intelligence. Intelligence 51, 10–27. https://doi.org/10.1016/j.intell.2015.04.009.

Cattell, R.B., 1963. Theory of fluid and crystallized intelligence: a critical experiment. J. Educ. Psychol. 54, 1–22. https://doi.org/10.1037/h0046743.

Cole, M.W., Bassett, D.S., Power, J.D., Braver, T.S., Petersen, S.E., 2014. Intrinsic and task-evoked network architectures of the human brain. Neuron 83, 238–251. https://doi.org/10.1016/j.neuron.2014.05.014.

Cole, M.W., Ito, T., Bassett, D.S., Schultz, D.H., 2016. Activity flow over resting-state networks shapes cognitive task activations. Nat. Neurosci. 19, 1718–1726. https://doi.org/10.1101/055194.

Colom, R., Karama, S., Jung, R.E., Haier, R.J., 2010. Human intelligence and brain networks. Dialogues Clin. Neurosci. 12, 489–501.

der Waerden, B.L., van der Waerden, B., 1952. Order tests for the two-sample problem and their power. Indag. Math. 14, 253–458. https://doi.org/10.1016/S1385-7258(52)50063-5.

Dubois, J., Adolphs, R., 2016. Building a science of individual differences from fMRI. Trends Cogn. Sci. 20, 1–19. https://doi.org/10.1016/j.tics.2016.03.014.

Dubois, J., Galdi, P., Han, Y., Paul, L.K., Adolphs, R., 2018. Resting-state functional brain connectivity best predicts the personality dimension of openness to experience. Personal. Neurosci. 1, e6. https://doi.org/10.1017/pen.2018.8.

Finn, E.S., Shen, X., Scheinost, D., Rosenberg, M.D., Huang, J., Chun, M.M., Papademetris, X., Todd Constable, R., 2015. Functional connectome fingerprinting: identifying individuals using patterns of brain connectivity. Nat. Neurosci. 18, 1–11. https://doi.org/10.1038/nn.4135.

Fox, M.D., Greicius, M., 2010. Clinical applications of resting state functional connectivity. Front. Syst. Neurosci. 4, 19. https://doi.org/10.3389/fnsys.2010.00019.

Geerligs, L., Rubinov, M., Cam-CAN, Henson, R.N., 2015. State and trait components of functional connectivity: individual differences vary with mental state. J. Neurosci. 35, 13949–13961. https://doi.org/10.1523/JNEUROSCI.1324-15.2015.

Glasser, M.F., Sotiropoulos, S.N., Wilson, J.A., Coalson, T.S., Fischl, B., Andersson, J.L., Xu, J., Jbabdi, S., Webster, M., Polimeni, J.R., Van Essen, D.C., Jenkinson, M., 2013. The minimal preprocessing pipelines for the Human Connectome Project. Neuroimage 80, 105–124. https://doi.org/10.1016/j.neuroimage.2013.04.127.

Gottfredson, L.S., 1997. Why g matters: the complexity of everyday life. Intelligence 24, 79–132. https://doi.org/10.1016/S0160-2896(97)90014-3.

Haier, R.J., Colom, R., Schroeder, D.H., Condon, C.A., Tang, C., Eaves, E., Head, K., 2009. Gray matter and intelligence factors: is there a neuro-g? Intelligence 37, 136–144. https://doi.org/10.1016/j.intell.2008.10.011.

Hearne, L.J., Mattingley, J.B., Cocchi, L., 2016. Functional brain networks related to individual differences in human intelligence at rest. Sci. Rep. 6, 32328. https://doi.org/10.1038/srep32328.

Hotelling, H., 1936. Relations between two sets of variates. Biometrika 28, 321–377.

Jung, R.E., Haier, R.J., 2007. The parieto-frontal integration theory (P-FIT) of intelligence: converging neuroimaging evidence. Behav. Brain Sci. 30, 135–154. https://doi.org/10.1017/S0140525X07001185.

Kettenring, J.R., 1971. Canonical analysis of several sets of variables. Biometrika 58, 433–451.

Lerman-Sinkoff, D.B., Sui, J., Rachakonda, S., Kandala, S., Calhoun, V.D., Barch, D.M., 2017. Multimodal neural correlates of cognitive control in the Human Connectome Project. Neuroimage. https://doi.org/10.1016/j.neuroimage.2017.08.081.

Modi, S., Kumar, M., Kumar, P., Khushu, S., 2015. Aberrant functional connectivity of resting state networks associated with trait anxiety. Psychiatry Res. Neuroimaging. 234, 25–34. https://doi.org/10.1016/j.pscychresns.2015.07.006.

Noble, S., Spann, M.N., Tokoglu, F., Shen, X., Constable, R.T., Scheinost, D., 2017. Influences on the test-retest reliability of functional connectivity MRI and its relationship with behavioral utility. Cerebr. Cortex 27, 5415–5429. https://doi.org/10.1093/cercor/bhx230.

Power, J.D., Barnes, K.A., Snyder, A.Z., Schlaggar, B.L., Petersen, S.E., 2012. Spurious but systematic correlations in functional connectivity MRI networks arise from subject motion. Neuroimage 59, 2142–2154. https://doi.org/10.1016/j.neuroimage.2011.10.018.

Raichle, M.E., 2015. The brain's default mode network. Annu. Rev. Neurosci. 38, 433–447. https://doi.org/10.1146/annurev-neuro-071013-014030.

Rosenberg, M.D., Finn, E.S., Scheinost, D., Papademetris, X., Shen, X., Constable, R.T., Chun, M.M., 2016. A neuromarker of sustained attention from whole-brain functional connectivity. Nat. Neurosci. 19, 165–171. https://doi.org/10.1038/nn.4179.

Schultz, D.H., Cole, M.W., 2016. Higher intelligence is associated with less task-related brain network reconfiguration. J. Neurosci. 36, 8551–8561. https://doi.org/10.1523/JNEUROSCI.0358-16.2016.

Shen, X., Tokoglu, F., Papademetris, X., Constable, R.T., 2013. Groupwise whole-brain parcellation from resting-state fMRI data for network node identification. Neuroimage 82, 403–415. https://doi.org/10.1016/j.neuroimage.2013.05.081.

Smith, S.M., Nichols, T.E., Vidaurre, D., Winkler, A.M., J Behrens, T.E., Glasser, M.F., Ugurbil, K., Barch, D.M., Van Essen, D.C., Miller, K.L., 2015. A positive-negative mode of population covariation links brain connectivity, demographics and behavior. Nat. Neurosci. 18, 1–7. https://doi.org/10.1038/nn.4125.

Smith, S.M., Vidaurre, D., Beckmann, C.F., Glasser, M.F., Jenkinson, M., Miller, K.L., Nichols, T.E., Robinson, E.C., Salimi-Khorshidi, G., Woolrich, M.W., Barch, D.M., Uğurbil, K., Van Essen, D.C., 2013. Functional connectomics from resting-state fMRI. Trends Cogn. Sci. 17, 666–682. https://doi.org/10.1016/j.tics.2013.09.016.

Takagi, Y., Sakai, Y., Abe, Y., Nishida, S., Harrison, B.J., Martínez-Zalacaín, I., Soriano-Mas, C., Narumoto, J., Tanaka, S.C., 2018. A common brain network among state, trait, and pathological anxiety from whole-brain functional connectivity. Neuroimage 172, 506–516. https://doi.org/10.1016/j.neuroimage.2018.01.080.

Takagi, Y., Sakai, Y., Lisi, G., Yahata, N., Abe, Y., Nishida, S., Nakamae, T., Morimoto, J., Kawato, M., Narumoto, J., Tanaka, S.C., 2017. A neural marker of obsessive-compulsive disorder from whole-brain functional connectivity. Sci. Rep. 7, 7538.

Tavor, I., Parker Jones, O., Mars, R.B., Smith, S.M., Behrens, T.E., Jbabdi, S., 2016. Task-free MRI predicts individual differences in brain activity during task performance. Science 352, 216–220. https://doi.org/10.1126/science.aad8127.

Uğurbil, K., Xu, J., Auerbach, E.J., Moeller, S., Vu, A.T., Duarte-Carvajalino, J.M., Lenglet, C., Wu, X., Schmitter, S., Van de Moortele, P.F., Strupp, J., Sapiro, G., De Martino, F., Wang, D., Harel, N., Garwood, M., Chen, L., Feinberg, D.A., Smith, S.M., Miller, K.L., Sotiropoulos, S.N., Jbabdi, S., Andersson, J.L.R., Behrens, T.E.J., Glasser, M.F., Van Essen, D.C., Yacoub, E., 2013. Pushing spatial and temporal resolution for functional and diffusion MRI in the Human Connectome Project. Neuroimage 80, 80–104. https://doi.org/10.1016/j.neuroimage.2013.05.012.

Van Essen, D.C., Ugurbil, K., Auerbach, E., Barch, D., Behrens, T.E.J., Bucholz, R., Chang, A., Chen, L., Corbetta, M., Curtiss, S.W., Della Penna, S., Feinberg, D., Glasser, M.F., Harel, N., Heath, A.C., Larson-Prior, L., Marcus, D., Michalareas, G., Moeller, S., Oostenveld, R., Petersen, S.E., Prior, F., Schlaggar, B.L., Smith, S.M., Snyder, A.Z., Xu, J., Yacoub, E., 2012. The Human Connectome Project: a data acquisition perspective. Neuroimage 62, 2222–2231. https://doi.org/10.1016/j.neuroimage.2012.02.018.

Via, J., Santamaria, I., Pérez, J., 2005. Canonical correlation analysis (CCA) algorithms for multiple data sets: Application to blind SIMO equalization. Signal Process. Conf. 1, 4–7.

Vía, J., Santamaría, I., Pérez, J., 2007. A learning algorithm for adaptive canonical correlation analysis of several data sets. Neural Netw. 20, 139–152. https://doi.org/10.1016/j.neunet.2006.09.011.

Winkler, A.M., Ridgway, G.R., Webster, M.A., Smith, S.M., Nichols, T.E., 2014. Permutation inference for the general linear model. Neuroimage 92, 381–397. https://doi.org/10.1016/j.neuroimage.2014.01.060.

Winkler, A.M., Webster, M.A., Vidaurre, D., Nichols, T.E., Smith, S.M., 2015. Multi-level block permutation. Neuroimage 123, 253–268. https://doi.org/10.1016/j.neuroimage.2015.05.092.